4-2018

Primary Atmospheric Drivers of Pluvial Years in the United States Great Plains

Paul Flanagan

Jeffrey B. Basara

Jason C. Furtado

Xiangming Xiao

Primary Atmospheric Drivers of Pluvial Years in the United States Great Plains

Paul X. Flanagan

School of Meteorology, University of Oklahoma, Norman, Oklahoma

Jeffrey B. Basara

School of Meteorology, and Oklahoma Climatological Survey, University of Oklahoma, Norman, Oklahoma

Jason C. Furtado

School of Meteorology, University of Oklahoma, Norman, Oklahoma

Xiangming Xiao

Department of Microbiology and Plant Biology, and Center for Spatial Analysis, University of Oklahoma, Norman, Oklahoma

(Manuscript received 2 August 2017, in final form 26 February 2018)

ABSTRACT

Precipitation variability has increased in recent decades across the Great Plains (GP) of the United States. Drought and its associated drivers have been studied in the GP region; however, periods of excessive precipitation (pluvials) at seasonal to interannual scales have received less attention. This study narrows this knowledge gap with the overall goal of understanding GP precipitation variability during pluvial periods. Through composites of relevant atmospheric variables from the ECMWF twentieth-century reanalysis (ERA-20C), key differences between southern Great Plains (SGP) and northern Great Plains (NGP) pluvial periods are highlighted. The SGP pluvial pattern shows an area of negative height anomalies over the southwestern United States with wind anomalies consistent with frequent synoptic wave passages along a southward-shifted North Pacific jet. The NGP pattern during pluvial periods, by contrast, depicts anomalously low heights in the northwestern United States and an anomalously extended Pacific jet. Analysis of daily heavy precipitation events reveals the key drivers for these pluvial events, namely, an east–west height gradient and associated stronger poleward moisture fluxes. Therefore, the results show that pluvial years over the GP are likely driven by synoptic-scale processes rather than by anomalous seasonal precipitation driven by longer time-scale features. Overall, the results present a possible pathway to predicting the occurrence of pluvial years over the GP and understanding the causes of GP precipitation variability, potentially mitigating the threats of water scarcity and excesses for the public and agricultural sectors.

1. Introduction

Precipitation is a critical asset for extensive agriculture across the Great Plains (GP) of the United States (Fischer et al. 2007). The GP of the United States (herein defined as the states of Texas, Oklahoma, Kansas, Nebraska, South Dakota, and North Dakota) possesses a unique precipitation climatology in that the climatological maxima of rainfall and temperature are asynchronous and occur at different times of the plant-growing season (Flanagan et al. 2017). Thus, if a precipitation deficit occurs during the time of year in which temperatures are climatologically at their maximum, the water stress on crops and the surface is dramatically increased. While irrigation can offset the impact of this water stress, conditions that bring about precipitation deficits typically cause abnormal temperature patterns, and further crop damage can still occur (e.g., Wilhite 2000; Wilhelmi and Wilhite 2002; Hoerling et al. 2014; Yin et al. 2014; Livneh and Hoerling 2016). Thus, precipitation deficits and excesses are critically important for the GP.

The GP is also a region of high precipitation variability across multiple spatial and temporal scales (e.g., Ting and Wang 1997; Ruiz-Barradas and Nigam 2005; Flanagan et al. 2017). Droughts occur with enough

Corresponding author: Paul Flanagan, pxf11@ou.edu

DOI: 10.1175/JHM-D-17-0148.1

frequency that numerous studies have investigated the drivers of such events within the GP region (Basara et al. 2013). A majority of these studies focused on the connections between various sea surface temperature (SST) patterns and their influence on anomalous synoptic flow patterns and consequently GP precipitation (e.g., Trenberth and Branstator 1992; Schubert et al. 2004; Seager et al. 2005; Cook et al. 2008; Seager and Hoerling 2014). Aside from SST patterns, other forcing mechanisms contributing to drought in the GP region include internal atmospheric variability (Seager et al. 2014) and land–atmosphere coupling (Mo et al. 1997; Koster et al. 2000; Schubert et al. 2004).

Conversely, periods of enhanced precipitation (i.e., pluvials) have been less examined despite similar (or even worse) negative socioeconomic impacts of these events such as mismanagement of water resources (Cook et al. 2011; Pederson et al. 2013), increased risk of floods or increased flood intensity (Pal and Eltahir 2002; Illston et al. 2004), and increased risk of wildfire in later years through buildup of biomass during the pluvial year (Westerling et al. 2003, 2006). Yet, to gain a full understanding of precipitation variability across the GP, both pluvial and drought periods must be examined and quantified. Most investigations into pluvial periods have assumed that they are driven by conditions opposite to that of drought and are thus focused on the influence of global SSTs on synoptic flow patterns similar to drought events (Yang et al. 2007; Schubert et al. 2008; Hu and Huang 2009; Cook et al. 2011). Hu and Huang (2009) found that GP precipitation anomalies are modified when phase alignment occurred between the Pacific decadal oscillation (PDO) and El Niño–Southern Oscillation (ENSO), with enhanced forcing for wet periods if PDO and ENSO were both in their warm phases and vice versa for their cold phases. Conversely, Cook et al. (2011) determined that tropical Pacific SST anomalies had little explanatory power during the central and western United States 1905–17 pluvial period and instead attributed the pluvial period to internal atmospheric variability. Moreover, Mo et al. (1997) illustrated the nonlinearity in the associated precursor patterns associated with pluvial and drought events over the GP during the summertime. They found that differences in eddy activity and subsequent moisture transport over the GP were key to the pluvial event. Trenberth and Guillemot (1996) found that differences in the North Pacific jet stream, eddy activity along the Pacific–North American storm track and moisture transport into the GP were the key differences between the 1993 floods and 1988 drought over the central United States. These past studies on pluvial events have focused primarily on single events, and a more comprehensive analysis of many events spanning multiple decades remains to be done.

The objective of our study is to use long-period (i.e., spanning the twentieth and twenty-first centuries) climatological reanalysis datasets to examine past pluvial periods in the GP of the United States and describe qualitatively and quantitatively the primary atmospheric drivers of such events. Along with filling a gap in the climate literature, this work will also contribute to emerging studies on the changing nature of GP precipitation both in the recent past (e.g., Christian et al. 2015; Weaver et al. 2016; Flanagan et al. 2017) and under future climate change (e.g., Rosenzweig et al. 2001; Dore 2005; Wuebbles et al. 2014).

2. Data and methods

a. *Datasets*

Long-term datasets are required for our comprehensive analysis of GP precipitation and relevant atmospheric variables. Precipitation data are from the Parameter-Elevation Regressions on Independent Slopes Model (PRISM; Daly et al. 2000), which provides monthly precipitation from 1895 to the present on a 4-km horizontal resolution. For atmospheric variables, we first consider two monthly reanalysis products: the National Oceanic and Atmospheric Administration/Cooperative Institute for Research in Environmental Sciences (NOAA/CIRES) Twentieth Century Reanalysis (20CR; Compo et al. 2011) and the European Center for Medium-Range Weather Forecasts (ECMWF) twentieth-century reanalysis (ERA-20C; Poli et al. 2016). Among these two reanalysis products, the ERA-20C dataset better reproduces the observed annual climatology of precipitation over the GP as depicted by PRISM (Fig. 1). In addition, ERA-20C produces a larger dataset of pluvial years for each composite compared to 20CR, especially when the northern Great Plains (NGP; i.e., North Dakota, South Dakota, and Nebraska) and southern Great Plains (SGP; i.e., Kansas, Oklahoma, and Texas) subregions are considered, which provides a more robust subset of the data to calculate the composite atmospheric fields. Thus, the 2° × 2° ERA-20C reanalysis dataset is selected to produce composites of atmospheric variables for this study and provides global coverage of all relevant atmospheric variables from 1926 to 2010 at various spatial resolutions, as precipitation data from ERA-20C is poor before 1926 (Poli et al. 2016). Mirroring previous pluvial studies, the analysis focuses on 500-mb (1 mb = 1 hPa) geopotential heights and 250-mb u and v wind components to identify specific atmospheric patterns found within pluvial

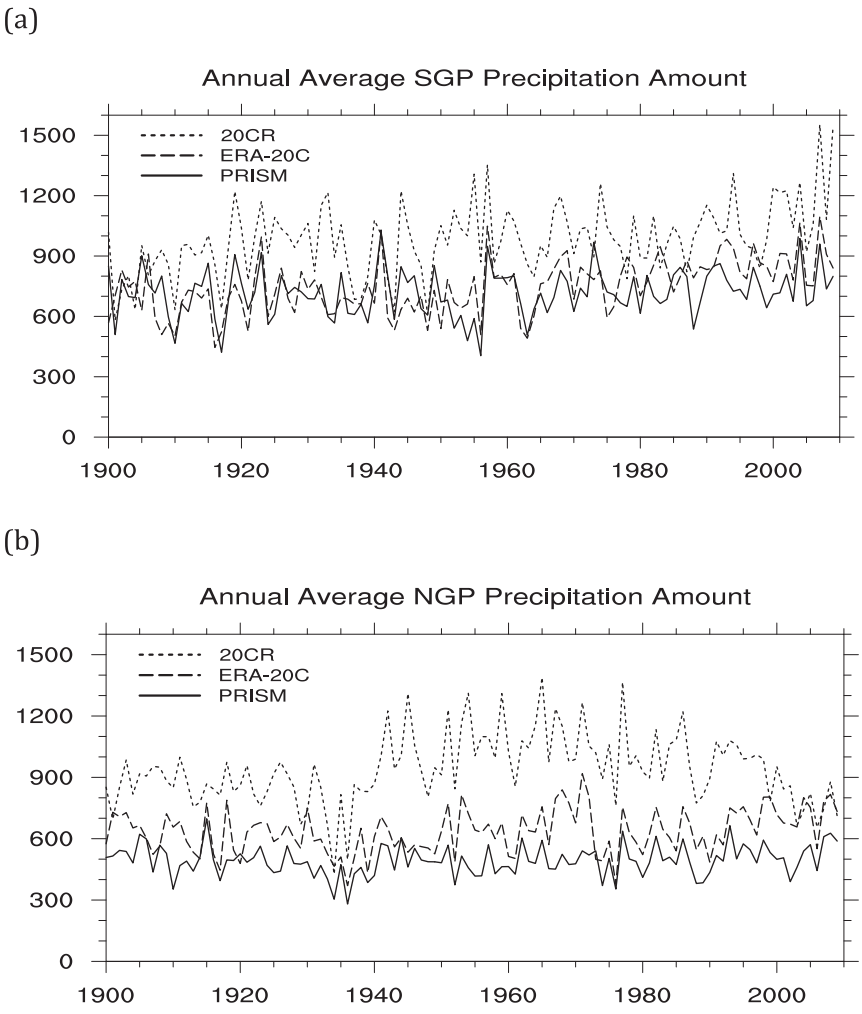

FIG. 1. The annual grid point average of the (a) SGP and (b) NGP precipitation amount from the PRISM (solid line), ERA-20C (long-dashed line), and 20CR (short-dashed line) datasets. The correlation between PRISM and ERA-20C in the SGP is 0.56 and 0.47 for 20CR. For the NGP, the correlation between PRISM and ERA-20C is 0.62, and for 20CR it is 0.38.

years in the NGP and SGP. Anomalies of these fields are derived by removing the mean of the 1926–2010 period. The inclusion of the NCEP–NCAR version 1 reanalysis (NCEP; Kalnay et al. 1996), 20CR, and the Japanese 55-year Reanalysis (JRA55; Onogi et al. 2007) serves to test the robustness of the results. All datasets are bilinearly interpolated to the same $2° \times 2°$ grid as ERA-20C for direct comparisons of the results.

b. Definition of pluvial periods

To determine GP pluvial events, we first divide the GP into two subregions: the NGP and the SGP. This division is completed because of distinct differences in precipitation variability between the SGP and NGP (Fig. 2; e.g., Christian et al. 2015; Weaver et al. 2016; Flanagan et al. 2017). Variability in the SGP is larger than that seen in the NGP, with a positive precipitation trend visible in ERA-20C more so than with PRISM (Fig. 2). For the NGP, both datasets have comparable trends and variance. Moreover, precipitation amounts are significantly higher for the SGP than the NGP, meaning that studying pluvial events for the entire GP would be unduly biased by SGP variability and totals. Therefore, we elect to explore pluvial events and their drivers in these two specific regions separately.

Next, a pluvial year for each subregion is identified if the calendar-year total precipitation is 10% greater than the climatological annual total precipitation in that subregion, that is,

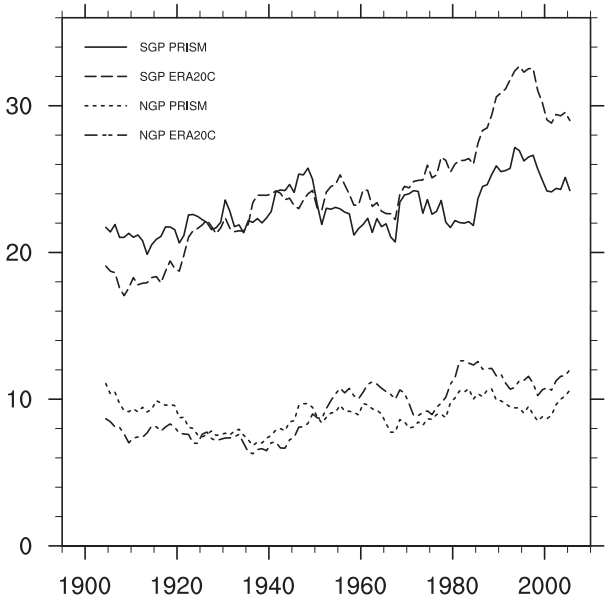

FIG. 2. The 10-yr running mean precipitation standard deviation (mm month^{-1}) for the PRISM and ERA-20C datasets. The solid (PRISM) and long-dashed (ERA-20C) lines represent the SGP and the short-dashed (PRISM) and long-and-short-dashed lines (ERA-20C) represent the NGP.

$$\frac{P_x}{P_y} \geq 1.1, \tag{1}$$

where P_x is the total annual precipitation amount of the given year, and P_y is equal to the average annual total from all (1926–2010) years. This definition is applied to all precipitation datasets, the list of all identified pluvial years is found in the appendix, and only years meeting the criterion in both PRISM and reanalysis products are used for composites analysis (Table 1). Sensitivity tests to other thresholds (e.g., 15%) yielded qualitatively similar results to those presented in this study (not shown).

Daily ERA-20C precipitation totals (i.e., accumulations from initialization at 0600 UTC until 0000 UTC) and atmospheric fields (i.e., geopotential height, zonal u and meridional v winds, and specific humidity q) taken at 0000 UTC are analyzed to determine the drivers of significant precipitation events during pluvial years. The 0000 UTC atmospheric fields are used rather than a daily mean for comparison with actual soundings (not shown). Because of the nonnormality of daily precipitation values, we use the 95th percentile of all precipitation events during pluvial years for defining a daily heavy precipitation event in each region. This methodology identified 275 events for the SGP and 274 events for the NGP.

c. Statistical methods

To facilitate the statistical analysis of the identified pluvial years for each region, composites were created using three primary atmospheric variables from ERA-20C: the 500-mb eddy geopotential height (EGH; i.e., removal of the zonal mean from the geopotential height field), u, and v. The EGH anomaly field represents the transient zonal inhomogeneities that distinguish wave features from the zonal-mean flow pattern (e.g., Randall 2015). Thus, EGH is a tool used to discern, separate, and analyze synoptic patterns that are responsible for weather events.

Several types of composites are explored in this work. First, we define "Total" composites as those composites resulting from using *all* pluvial years. However, such composite maps inherently hold a couple of limitations and caveats. First, composites may be unduly influenced by a small subset of extreme events within the total population. Second, owing to the impacts of climate change, both the mean and variance of GP precipitation have changed over the twentieth century (e.g., Fig. 1), introducing nonstationarity concerns into the data record. To address these issues, two additional composites are employed in this study:

- "Pattern" composites: These composites are created by selecting specific pluvial years that have spatial atmospheric patterns that closely match the spatial pattern in the Total composite (i.e., the "pattern" matches). To choose these specific pluvial years, we compute an index of the EGH anomaly field by projecting the EGH anomaly field for each year onto that obtained from the Total composite analysis. This index is computed for the two subregions in our study (10°–50°N, 130°–90°W for the SGP; 30°–50°N,

TABLE 1. List of years for each composite category that were defined as pluvial within the study for the ERA-20C dataset.

	SGP	NGP
Total	1926, 1941, 1957, 1968, 1974, 1979, 1987, 1990, 1991, 1992, 1997, 2002, 2004, 2007, 2009	1941, 1951, 1962, 1965, 1977, 1982, 1986, 1993, 1995, 1998, 2005, 2007, 2008, 2009, 2010
Pattern	1926, 1941, 1987, 1991, 1992, 1997, 2002, 2004	1951, 1982, 1998, 2008, 2010
Break	1926, 1941, 1957, 1959, 1961, 1968, 1974, 1979, 1992, 1997, 2004, 2007	1941, 1951, 1962, 1965, 1971, 1977, 1982, 1986, 1993, 1995, 1998, 2005, 2007, 2008, 2010

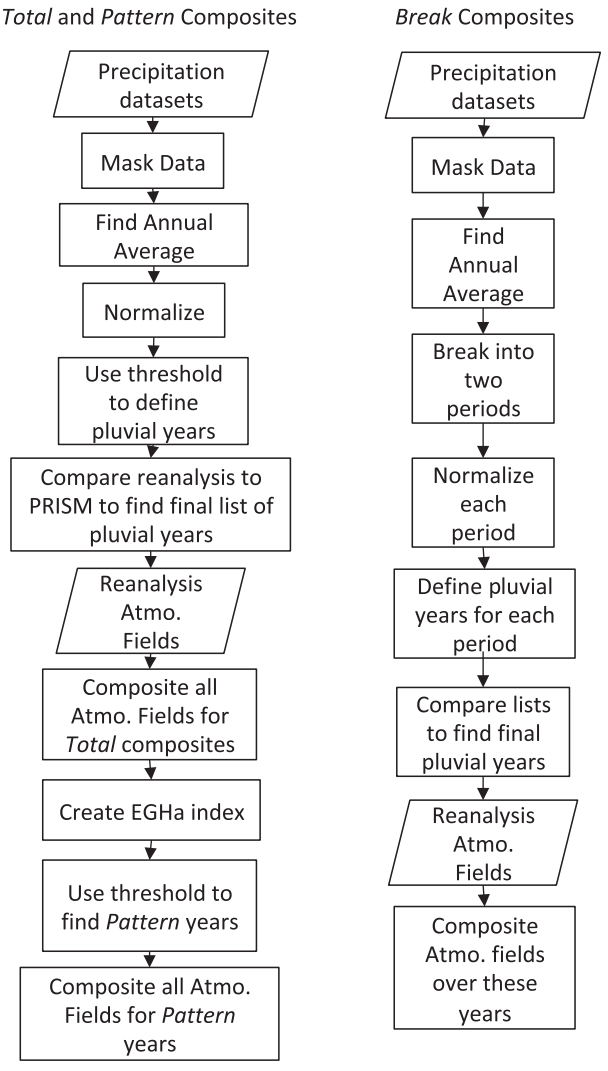

FIG. 3. Description of the workflow used to create each composite type. EGHa stands for EGH anomalies and "Atmo." is used in place of "atmospheric."

130°–90°W for the NGP). The EGH anomaly field is specifically chosen rather than the precipitation field itself because we are more interested in the atmospheric drivers responsible for pluvial years, not the specific precipitation spatial pattern. Years when the EGH anomaly index exceeded 0.5σ are designated as Pattern years and subsequently used for our Pattern composites. Using this methodology, 8 (5) pluvial years are used for the Pattern composites in the SGP (NGP) region. Additionally, 19 (17) nonpluvial years also featured EGH anomaly years that matched the atmospheric forcing patterns in the SGP (NGP). As such, the Pattern compositing method highlights those years that strongly influence the Total composite results along with identifying other years that deviate from the Total composites.

- "Break" composites: To examine the influence of nonstationarity on our results, we split the annual precipitation record into two distinct periods. The break point is objectively found by identifying the longest period (in years) where the standard deviations between the two are statistically significantly different ($p < 0.05$). Then, new means are computed for each of the two periods. These means form the basis for defining pluvial years in each Break period from (1). The Break pluvial years then form the basis for the Break composites of the atmospheric fields.

Figure 3 provides a flow diagram detailing the construction of these composite fields.

Composites for the heavy precipitation event analysis were created by averaging the 0000 UTC atmospheric fields over all days within pluvial years in which the daily precipitation amount crossed the 95th percentile. For the heavy precipitation event analyses, we also analyze moisture fluxes (i.e., $u'q'$ and $v'q'$, where the prime notation indicates deviations from the time mean). This additional metric is included to identify both source regions of moisture for the heavy precipitation events and the actual transport path. Furthermore, the moisture fluxes complement the EGH anomaly spatial patterns by explicitly showing how the synoptic-scale waves depicted in the EGH anomaly fields contribute to the heavy precipitation events.

Significance testing of all composites is done by taking 1000 random samples of the composited field (by grid point), with the same number of years as the composite and deriving 1000 resultant composites. The resulting 1000 bootstrapped composites are then used to define the two-tailed significance 90% threshold (e.g., Grotjahn and Faure 2008; Klingaman et al. 2008; Guo et al. 2017; Seo et al. 2017; Bukovsky et al. 2017) used to determine if the composite-mean value of the field at a specific grid point (chosen for pluvial analysis) is significantly different from choosing values at random. Because of the relatively small sample size of pluvial years, particularly for the Pattern composites, we elect to use the 90% significance threshold for all significance testing. As with many statistical studies of extreme events, the sample size can be relatively small, and we appropriately caveat our results because of that fact.

3. Results

a. Southern Great Plains pluvial analysis

The initial step in understanding the primary drivers of GP pluvial years is understanding the synoptic- and

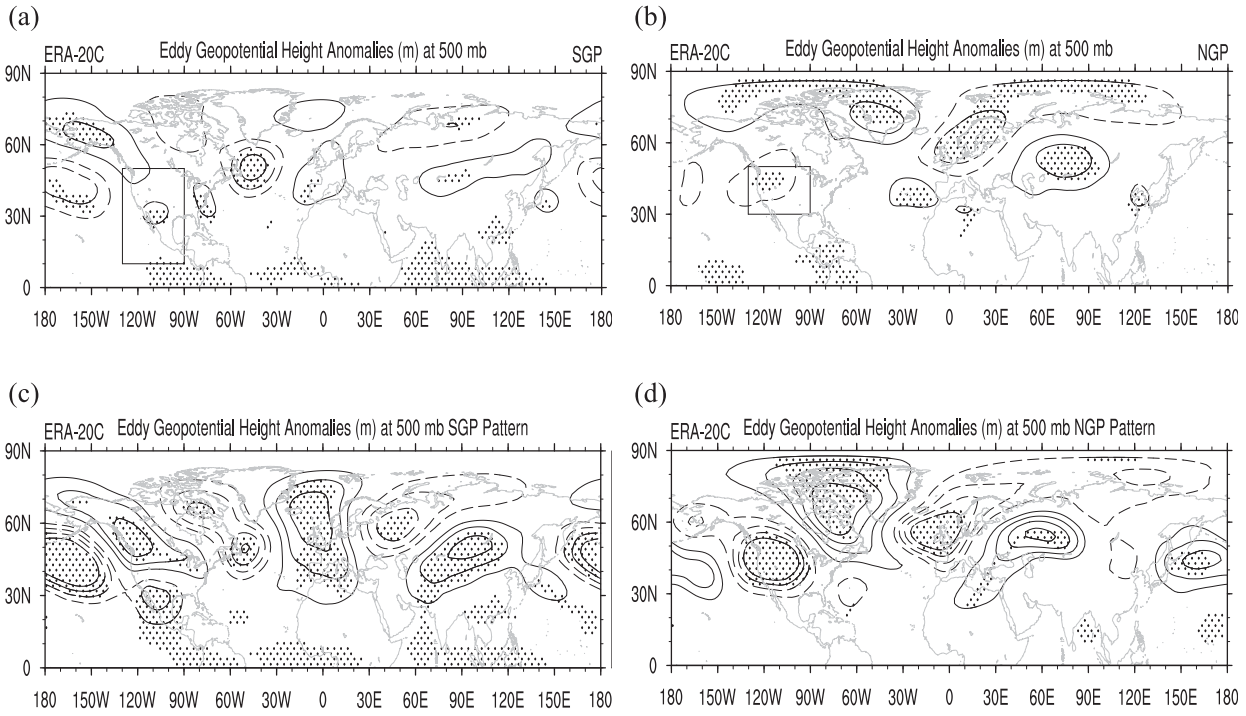

FIG. 4. The (top) Total (all Total pluvial years) and (bottom) Pattern (Pattern pluvial years) composites for the (a),(c) SGP and (b),(d) NGP. Contours are plotted from 16 to −16 m in intervals of 4 m without the 0-m contour. Statistically significant values at the 90% level are stippled. Negative contours are dashed, and solid contours represent positive values. The boxed regions in (a) and (b) represent the areas used to create the EGH anomaly index noted in Fig. 3.

larger-scale patterns that drive the excess precipitation. Here, "synoptic" refers to the spatial scale of the atmospheric fields and patterns studied—that is, structures and phenomena that are at least 1000 km in scale (i.e., the size of extratropical cyclones). The Total SGP EGH anomaly composites (Fig. 4a) depict a Rossby wave pattern over North America, with negative anomalies centered over the southwestern portion of the United States and south of Greenland with an area of positive anomalies over the northeastern United States. To better diagnose these patterns, years in which the 500-mb EGH anomaly field matched the Total composite anomaly height field across the southwestern portion of North America are also investigated. The Pattern composite (Fig. 4c) depicts a stronger negative anomaly signal occurring in the southwest extending farther to the northwest over the North Pacific Ocean. To further diagnose the differences in the wave structure for the Pattern years, we investigate the v (Fig. 5) and u (Fig. 6) anomaly fields. The 250-mb v wind component anomaly Pattern composite (Fig. 5a) exhibits a series of statistically significant (denoted by stippling in Fig. 5) couplets across Asia and North America, representing synoptic-scale waves, as synoptic wave patterns cause the flow to become anomalously meridional on their peripheries. The 250-mb u wind component anomaly Pattern composites (Fig. 6a) depict a southward displacement of the North Pacific jet during those years, with the center of the positive anomalies starting over eastern central Asia and stretching across the Pacific and negative anomalies to the north. This southward displacement of the jet facilitates the more active southern stream of the jet and thus heightens storm activity in the SGP, increasing the chances for heavy rainfall (Figs. 4a,c).

b Northern Great Plains pluvial analysis

Similar to the SGP analysis, we began the NGP investigation into the primary atmospheric patterns for NGP pluvial years with analysis of the EGH anomalies. The Total annual NGP EGH anomaly composite (Fig. 4b) shows an area of negative height anomalies over the northwestern United States. The NGP Pattern composites of EGH (Fig. 4d) show larger negative anomalies over the northwestern United States with an enlarged area of negative EGH anomalies extending northwestward toward the Aleutian Islands. Though not statistically significant, the negative EGH anomalies in

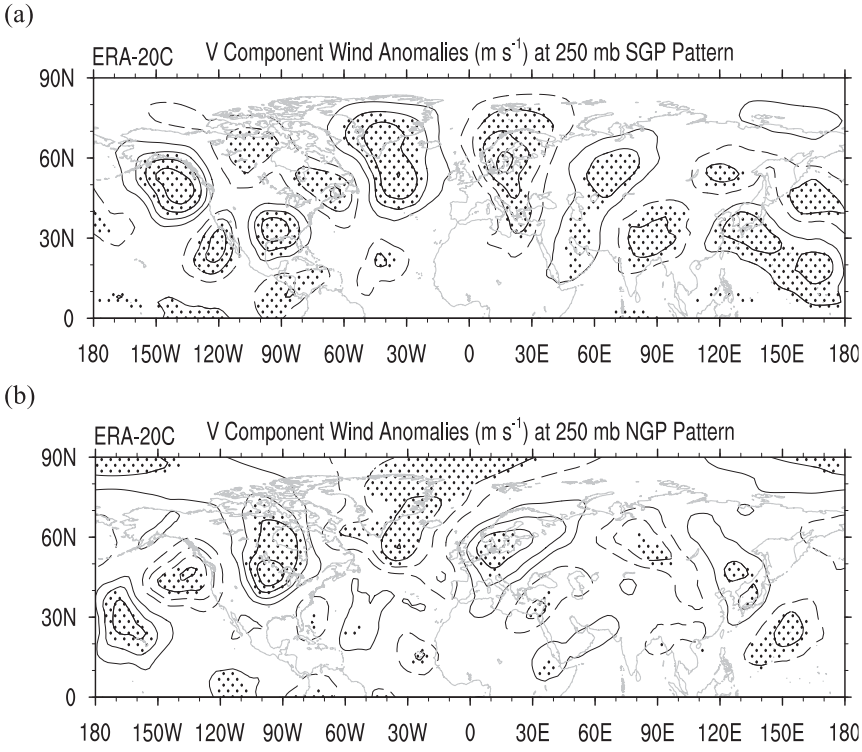

FIG. 5. The 250-mb v wind component anomalies for (a) SGP and (b) NGP Pattern years. Contours are plotted from 2 to $-2\,\mathrm{m\,s^{-1}}$ in intervals of $0.5\,\mathrm{m\,s^{-1}}$. Statistically significant values at the 90% level are stippled.

the North Pacific suggest that storm systems originating from the North Pacific near the Aleutian low produce the negative height anomalies in the northwestern United States. Analyses of NGP anomalous wind components (Figs. 5b, 6b) depict a much different pattern than that seen in the SGP composites. Statistically significant 250-mb v wind component anomalies are located farther northward and are less coherent in terms of a wave structure or pattern in the Pattern composites compared to the SGP Pattern composites (cf. Fig. 5b with Fig. 5a). Moreover, the 250-mb u anomalies exhibit positive anomalies over the central western coast of the United States extending up over the Aleutian Islands, representing with an extension of the North Pacific jet stream over the United States and thus facilitating more storm systems to traverse the NGP along this extended storm track (e.g., Griffin and Martin 2017).

c. *Robustness of the pattern composite results*

Because each reanalysis is run using a different dynamical core, parameterization configuration, vertical and horizontal resolution, etc., testing our results in other reanalysis datasets tests the robustness of our conclusions. For brevity, we will compare Pattern composites from ERA-20C with those from several other reanalysis datasets. For the SGP region (Fig. 7), the Pattern composites for each different reanalysis dataset depict a center of negative height anomalies over the southwestern United States. Despite small differences in the details of the negative anomalies, the different reanalyses largely agree on the general EGH anomaly pattern shown for ERA-20C (i.e., Fig. 4). This is generally true for the NGP as well (not shown), except for the JRA-55 dataset. For JRA-55, not a single year emerged for analysis in the Pattern composite. Part of this lack of samples arises because of the scarcity of pluvial years identified within the JRA-55 dataset for the NGP in particular. Curiously, the JRA55 reanalysis capably supplied years for the Pattern composites for the SGP, suggesting that this reanalysis may not depict salient features of NGP precipitation variability. Despite this one discrepancy, we conclude that our results remain robust and statistically significant independent of the reanalysis product chosen.

d. *Heavy precipitation event analysis*

To determine the drivers of heavy precipitation during pluvial years, composites of daily heavy precipitation events during pluvial years are examined. The EGH

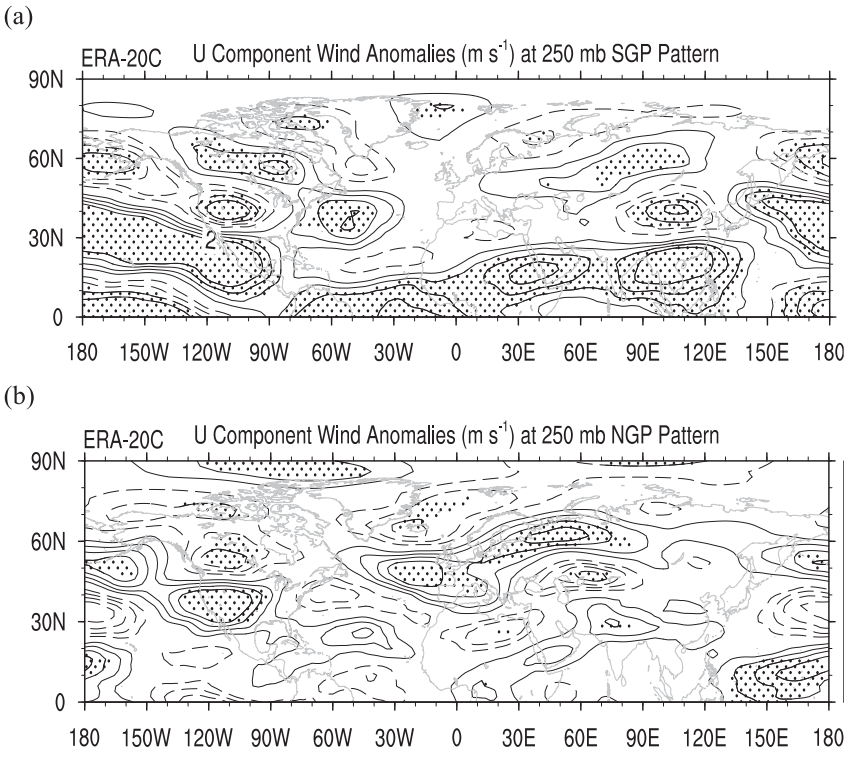

FIG. 6. The 250-mb u wind component anomalies for (a) SGP and (b) NGP Pattern years. Contours are plotted from 2 to -2 m s^{-1} in intervals of 0.5 m s^{-1}. Statistically significant values at the 90% level are stippled.

anomalies for the SGP (Fig. 8a) and NGP (Fig. 8b) show a significant height dipole across the United States with negative (positive) height anomalies in the west (east). Differences between the two subregions emerge in terms of the location and strength of the negative dipole. In particular, the SGP composite indicates weaker negative anomalies centered over southeastern New Mexico versus a strong negative node over northwestern Colorado in the NGP composite (Fig. 8). More importantly, the EGH anomaly patterns also allude to differences in moisture fluxes ($u'q'$, $v'q'$) between these two regions (Fig. 9). The magnitude of differences in these fluxes is particularly important for NGP heavy precipitation events because of the distance between the primary moisture source (e.g., Gulf of Mexico) and the northern extent of the GP. To show this, analysis of the 925-mb net moisture flux averaged over the GP (24°–50°N, 106°–84°W) during each region's heavy precipitation events was calculated and compared. Moisture flux anomaly values for the NGP ($963.3\,\mathrm{m\,s^{-1}\,g\,kg^{-1}}$) were 14% higher compared to the SGP ($840.7\,\mathrm{m\,s^{-1}\,g\,kg^{-1}}$) net flux anomalies during the pluvial year heavy precipitation events and 15% higher than the climatological value of the moisture flux anomalies over the GP ($831.2\,\mathrm{m\,s^{-1}\,g\,kg^{-1}}$). However, the moisture flux anomalies are still largely positive during SGP heavy precipitation events, showing that enhanced moisture fluxes play a role in heavy precipitation events across the entire GP.

e. *Break composites*

Finally, we investigate the role that nonstationarity in precipitation statistics may be playing in our pluvial year composites. As described in section 2, we analyze the standard deviation of SGP and NGP precipitation separately to determine if different regimes of variability exist within the long data region. A statistically significant difference in standard deviations in both regions appears in 1980, and so 1980 is considered a "break point" or regime shift point for our pluvial analyses. The subsequent results of the Break composites (Fig. 10) reveal highly similar EGH anomaly patterns observed for the Total composites (Figs. 4a,b) for the SGP and the NGP. While small differences in the location and size of the important anomaly centers are apparent, differences are statistically insignificant via Monte Carlo simulations. Additionally, analysis of 250-mb u and v anomalies for the Break composites (not shown) are also similar to those in the Total composites. These similarities are somewhat

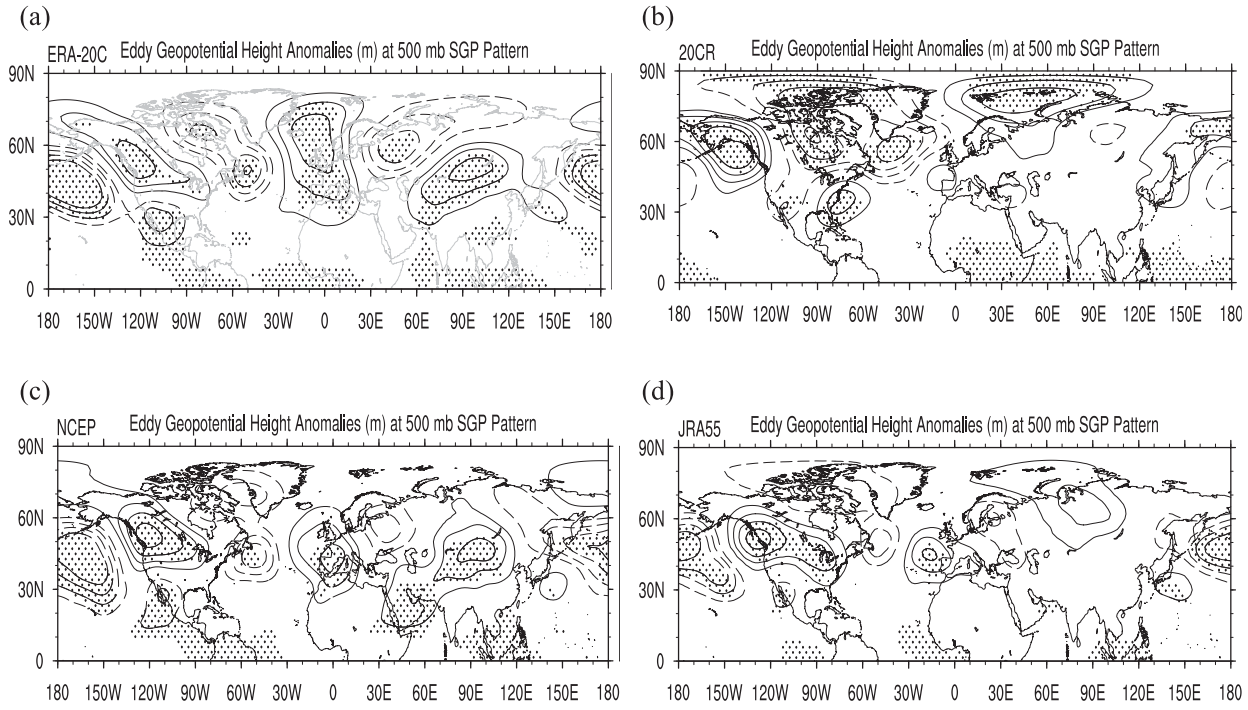

FIG. 7. EGH anomaly SGP Pattern composites for (a) ERA-20C, (b) 20CR, (c) NCEP, and (d) JRA55. Contours are plotted from 16 to −16 m in intervals of 4 m, and statistically significant values at 90% are stippled. Negative contours are dashed, and solid contours represent positive values. All datasets were analyzed on a 2° × 2° grid.

expected—there are overlapping years included within the Total and Break composites (Table 1). More specifically, two years (1961 and 1974) are added to the SGP Break composite compared to the Total composite years used but five years (1987, 1990, 1991, 2002, and 2009) are removed, Likewise, one year (2009) is removed and one (1971) added to the NGP Break composite sample versus the NGP Total composite sample. Taken together, we conclude that nonstationarity in the GP precipitation time series has minimal impact on the results of this analysis.

4. Discussion

The results presented in this work highlight the primary atmospheric drivers responsible for high rainfall years over the NGP and SGP separately. However, several other key conclusions arise when considering all composites collectively. Starting in the SGP, u anomalies associated with pluvial years (Fig. 6a) suggest that the Pacific waveguide is displaced equatorward more frequently than during nonpluvial years. This waveguide is an important feature of the atmosphere over the Pacific and North America region as it facilitates the passage of eastward-traveling synoptic waves toward North America (Branstator and Teng 2017; see also Figs. 4a,c). The southward shift of the storm track would also allow for enhanced moisture transport into the SGP as the storms can more readily tap into moisture-rich sources in the lower midlatitudes of the Pacific. This anomalous southward shift of the Pacific waveguide is further supported by the uniformity of the v anomalies and strongly negative EGH anomalies seen in the daily heavy precipitation event analysis (Fig. 8a). Thus, enhanced synoptic activity over the southwestern United States is a hallmark trait for pluvial periods in the SGP. Furthermore, the southwestern United States is also a climatological hotspot for cutoff lows—that is, persistent areas of low pressure/geopotential heights displaced from the main jet stream and thus "stuck" or "cut off" from the large-scale zonal flow pattern—especially during the warm season (April–September). These systems typically induce instability and therefore precipitation and even severe convective events (Nieto et al. 2005). The "closed contour" nature of the negative height anomalies over the southwestern United States seen in the Total and Pattern composites (Figs. 4a,c) are suggestive of these cutoff low features.

While the frequency of synoptic waves and precipitation events appears important for SGP pluvial years, the intensity of the synoptic waves are the important factor for NGP pluvial years. Evidence for this

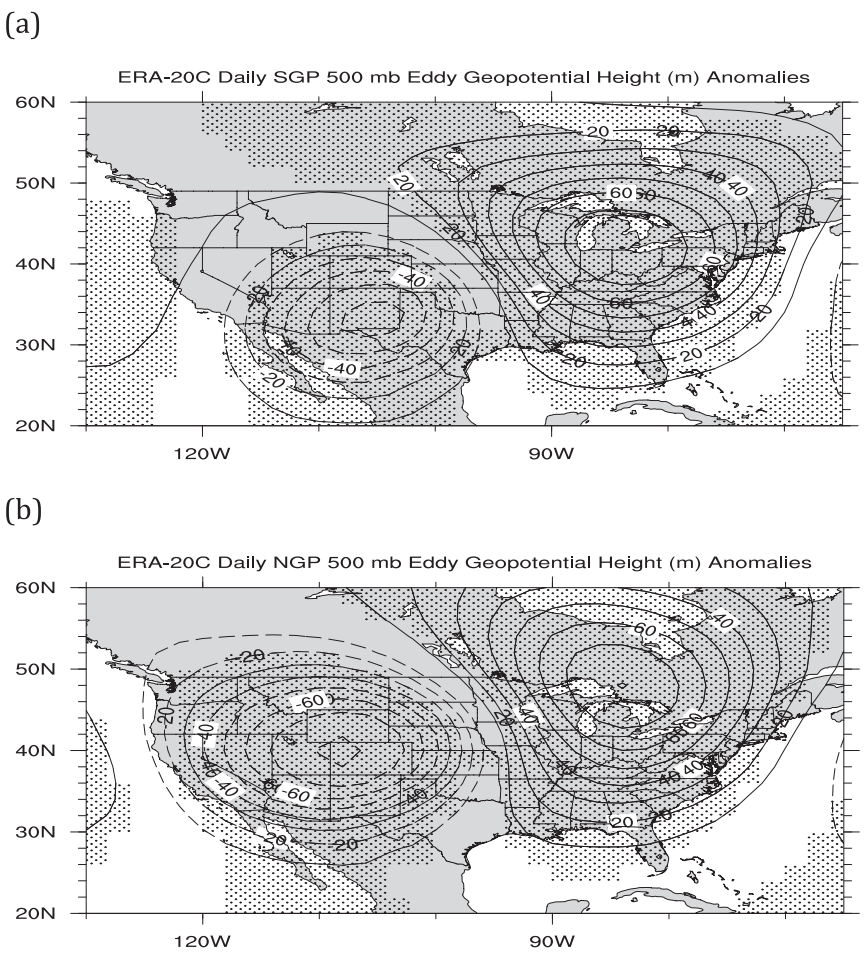

FIG. 8. Composite 500-mb EGH anomalies (m) for daily heavy rain events for the (a) SGP and (b) NGP. Contours are from −80 to 80 m with intervals of 10 m, and values that are statistically significant at the 90% level are stippled. Negative contours are dashed, and solid contours represent positive values.

conclusion includes larger negative EGH anomalies in the NGP Total and Pattern composites (Figs. 4b,d) and the daily heavy precipitation analysis composites (Fig. 8b) compared to the counterpart SGP composites (Figs. 4a, 4c, and 8a) Moreover, the magnitude of the NGP moisture flux anomalies during heavy precipitation events correlates with stronger extratropical cyclone activity, as deeper and more intense storms have stronger cyclonic flow that can transport more moisture farther inland. Indeed, because the NGP is located much farther away from the key source of moisture for heavy precipitation events than areas of the SGP, these stronger fluxes are necessary. Without these deep troughs over the north-central United States, moisture transport would be insufficient to provide the necessary precipitable water necessary for such heavy rainfall events. Additionally, the EGH anomalies analyzed for NGP pluvial years (Figs. 4b,d) influence the atmospheric pattern in other ways, including acting as an eastward extension of the Pacific jet stream. As the jet stream is the main waveguide or pathway for synoptic storms to travel, a jet extension toward North America favors more propagation of synoptic waves over central North America, resulting in the EGH anomalies in the Total and Pattern composites. Feedbacks between the waves and the large-scale flow are also important to consider for jet extension regimes. For example, while an extended jet allows for more synoptic wave activity, that enhanced wave activity both extracts *and* returns kinetic energy to the large-scale mean flow. Therefore, the more intense extratropical cyclones could reinforce the extended jet regime and thus contribute positively to the extreme rainfall events in the NGP. This feedback aspect is beyond the scope of this work but is interesting to consider.

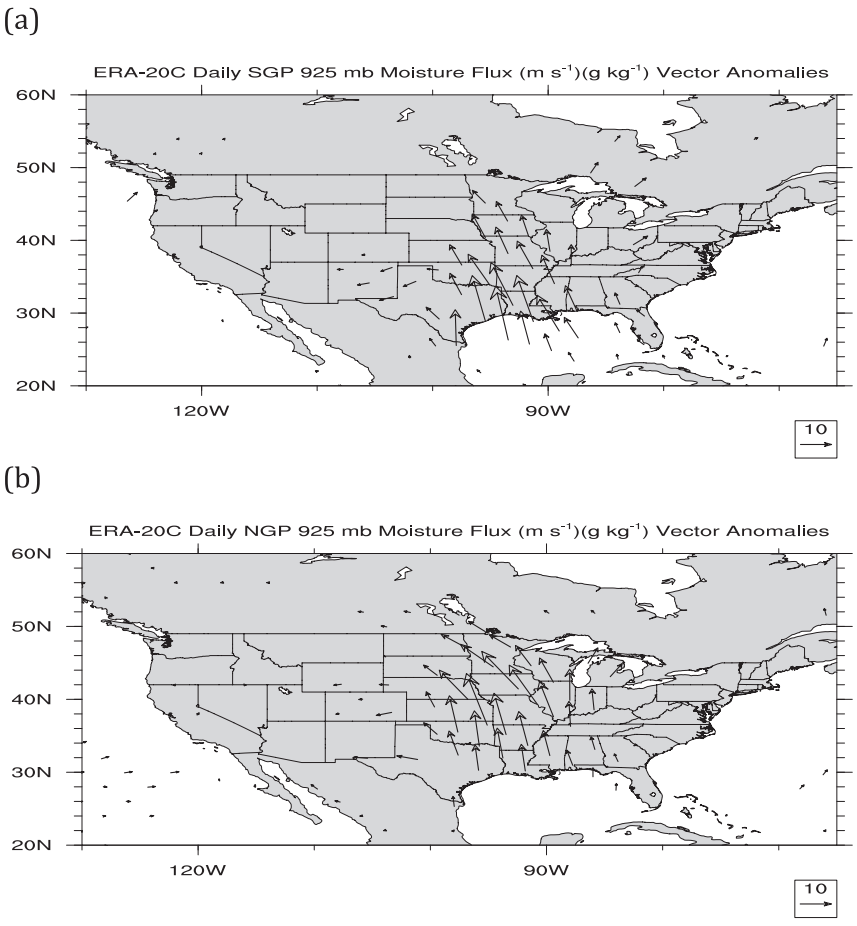

FIG. 9. Composite 925-mb moisture flux ($u'q'$, $v'q'$) anomaly vectors ($m\,s^{-1}\,g\,kg^{-1}$) for daily heavy rain events for the (a) SGP and (b) NGP. The standard vector length was used for a vector magnitude of $10\,m\,s^{-1}\,g\,kg^{-1}$, and vectors that are statistically significant at the 90% level are plotted.

Last, most of our analysis has focused on extratropical midlatitude variability and its impact on heavy rainfall in the GP on an annual basis. However, other remote forcings from global SSTs (e.g., Hu and Huang 2009; Cook et al. 2011) and anomalous tropical convection in the west Pacific warm pool (e.g., Barsugli and Sardeshmukh 2002) are also contributors to pluvial rainfall patterns in the GP. The Pacific jet stream, identified in this study as an important conduit for the extratropical cyclones impacting the GP rainfall, can also be modulated (in strength and position) from the Madden–Julian oscillation (MJO; e.g., Moore et al. 2010). Moreover, these remote impacts are also seasonally dependent, and thus the seasonality of GP pluvial events remains an open question for future work.

5. Conclusions

The primary large-scale atmospheric drivers of pluvial years over the Southern Great Plains (SGP) and Northern Great Plains (NGP) were investigated via composite analysis of atmospheric reanalysis products. The goal of this study was to generalize previous works on Great Plains (GP) pluvial periods, which focused on specific pluvial events, and develop a more meteorological framework of understanding of GP precipitation variability. Subsetting our pluvial years into the Pattern and Break composite analyses illustrated that 1) the associated atmospheric patterns are indeed features of the pluvial years and not an artifact of extreme events in the Total composites, and 2) changing statistics of GP precipitation have minimal impact on the atmospheric driving patterns identified in this study. Our results were tested with several atmospheric datasets and found to be robust findings, adding confidence to the conclusions we draw from this work (e.g., Fig. 7).

The study yielded two distinct annual-mean atmospheric patterns that are linked to pluvial events in the subregions of the GP. The SGP pluvial pattern consists

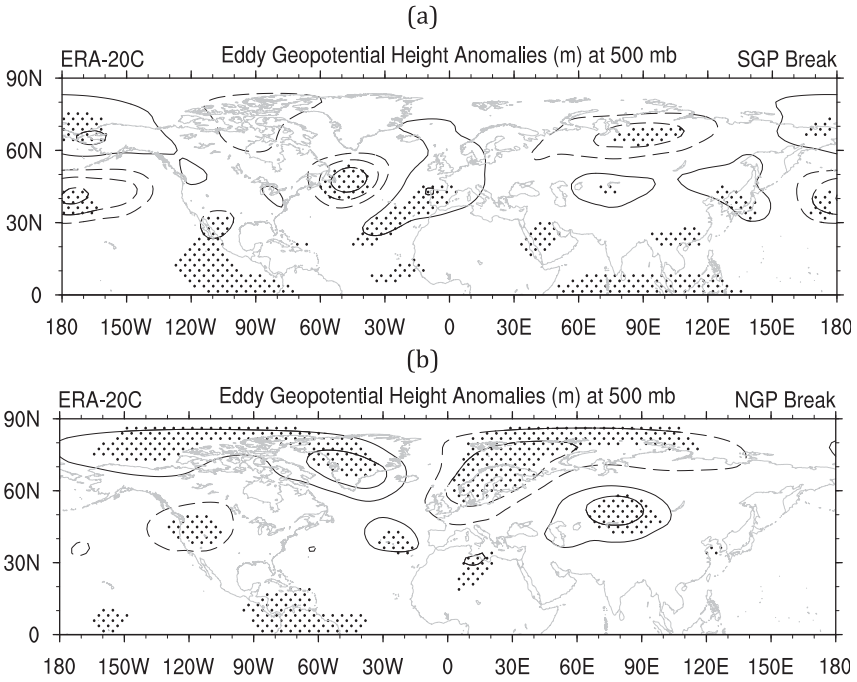

FIG. 10. Break (all Break pluvial years) composites for 500-mb EGH anomalies (m) for the (a) SGP and (b) NGP. Contours are from −20 to 20 m with intervals of 4 m, and values that are statistically significant at the 90% are stippled. Negative contours are dashed, and solid contours represent positive values.

of a closed area of negative height anomalies across the southwestern United States, with the wind anomalies showing a coherent hemispheric wave train pattern and an enhanced southward shift in the jet stream associated with the passage of storm systems (Figs. 4a,c). This pattern would lead to enhanced moisture flow from the south within the boundary layer leading to a higher chance of heavy precipitation (Fig. 8a). However, enhanced moisture transport is not *necessary* to drive pluvial years, but rather an increase in the number of precipitation events themselves. The lack of a relevant intensity signal in moisture fluxes in the SGP is likely due to the larger variability in precipitation in the SGP (Fig. 2) and thus the propensity for heavy precipitation events in the SGP from year to year. The pattern of EGH anomalies analyzed through the Pattern composite analysis is a common feature in daily heavy precipitation events over the SGP (Zhao et al. 2017) and is seen in the daily heavy precipitation event results as well.

The NGP pattern features negative height anomalies over the northwestern United States and southern Canada with an eastward extension of the North Pacific jet (Figs. 4b,d). The NGP EGH pattern is consistent with enhanced moisture advection into the NGP (Fig. 8b). This jet extension aids in the propagation of synoptic waves toward the NGP region. The NGP v wind anomalies (Fig. 5b) depict a pattern of couplets across the northern United States; however, the pattern is less coherent than in the SGP composites and regionally confined. Thus, the passage of more amplified synoptic waves over the northern United States, rather than the occurrence of frequent synoptic events important to SGP pluvial years, likely drives the heavy precipitation during NGP pluvial years. These stronger storm systems also provide enhanced moisture transport from the Gulf of Mexico, produced by deeper troughs, which drives excess precipitation during these years. The difference in synoptic activity can be seen in the daily heavy precipitation analysis, as comparisons between the SGP and NGP results (Fig. 8) show that the magnitude of the EGH anomalies in the NGP are higher than that of the SGP anomalies.

From a meteorological standpoint, the results presented in this work detail a complex atmospheric pattern that is the initial step in understanding the wet side of GP precipitation variability. From a water resources standpoint, the work details a pathway to understanding the processes that bring excess water to the region. Though the study represents an initial step in diagnosing these atmospheric patterns responsible for pluvial years over the GP, it offers a potential pathway of predictability on seasonal or longer time scales for excess precipitation periods over the region. As of now, such

TABLE A1. List of all pluvial years for the SGP and NGP found in each of the datasets considered. Bold years are pluvial years that match with observed (PRISM) pluvial years. The length of the period for each dataset is located below the dataset's name.

Pluvial Years SGP					Pluvial Years NGP				
ERA-20C 1900–2010 (15)	20CR 1851–2014 (10)	NCEP 1949–2016 (13)	JRA55 1958–2013 (11)	PRISM 1895–2016	ERA-20C 1900–2010 (15)	20CR 1851–2014 (10)	NCEP 1949–2016 (11)	JRA55 1958–2013 (4)	PRISM 1895–2016
2009	**2009**	2016	**2009**	2015	**2010**	2012	**2013**	**1995**	2015
2008	**2007**	**2015**	**2007**	2009	**2009**	**2011**	**2011**	**1993**	2014
2007	**2004**	2010	**2004**	2007	**2008**	**1993**	**2010**	1991	2013
2004	**2002**	**2007**	1993	2004	**2007**	1991	**2008**	**1986**	2011
2002	2001	**2004**	**1992**	2002	**2005**	**1986**	**2005**	1984	2010
2001	2000	**2002**	**1991**	1997	2004	1985	**1998**	1983	2009
1999	1994	**1997**	**1990**	1992	2000	1984	1997	**1982**	2008
1998	**1990**	1995	**1987**	1991	1999	**1982**	1996	1975	2007
1997	**1974**	**1991**	**1986**	1990	**1998**	**1977**	**1995**		2005
1994	**1968**	**1987**	**1985**	1987	**1995**	1975	**1993**		1998
1993	1967	**1986**	**1981**	1986	1994	1971	1991		1995
1992	**1960**	1984	**1973**	1985	**1993**	1968	**1986**		1993
1991	**1957**	1983		1981	**1986**	1967	**1982**		1986
1990	1955	**1981**		1979	**1982**	**1965**	**1977**		1982
1989	1952	**1973**		1974	**1977**	1964	1975		1977
1987	**1944**	**1968**		1973	1972	**1962**	1973		1965
1984	1933	**1957**		1968	1971	1959	1972		1962
1983	1932	1955		1961	1969	**1957**	1971		1957
1982		**1949**		1960	1968	1956	1970		1951
1979				1959	1967	1954	1969		1946
1978				1958	**1965**	1953	1968		1942
1974				1957	**1962**	**1951**			1941
1971				1949	1954	1945			1927
1969				1946	1953	**1942**			
1968				1944	**1951**				
1967				1942	1941				
1957				1941	1930				
1941				1935					
1926				1926					

long-range precipitation forecasts from the NOAA Climate Prediction Center, for example, rely on statistical models relating SST, trends, and other long-timescale signals over the United States (e.g., O'Lenic et al. 2008). Our results set new benchmarks to explore in terms of atmospheric patterns that could lead to more skillful predictors for GP pluvial periods.

Understanding GP precipitation variability is a difficult challenge, from the lack of previous research into all facets of this variability (Cook et al. 2011) to the multifaceted drivers of precipitation over the region such as land–atmosphere interactions (Mo et al. 1997; Koster et al. 2000; Schubert et al. 2004), internal atmospheric variability (Ruiz-Barradas and Nigam 2005; Seager et al. 2014), and climate teleconnections (e.g., Trenberth and Branstator 1992; Schubert et al. 2004; Seager et al. 2005; Cook et al. 2008; Seager and Hoerling 2014). However, variability of water resources is important to the region as agriculture is a dominant component of the regional economy (Fischer et al. 2007). Thus, increasing our understanding of the causes of GP precipitation variability is key to successfully managing and maintaining the socioeconomic and ecosystem success of the GP region.

The results presented in this study advance our knowledge in understanding one facet of the GP precipitation variability that has largely gone unstudied. Previous studies have investigated pluvial/flood cases (Trenberth and Guillemot 1996; Cook et al. 2011) and pluvials on seasonal time scales (Mo et al. 1997; Hu and Huang 2009) with a focus on eddy frequency and intensity, moisture flux, flow patterns, and associated climate patterns. Our results largely agree with their findings—enhanced synoptic wave activity, either in terms of frequency (SGP) or intensity (NGP), enhanced moisture transport during precipitation events, and anomalous flow patterns over the northern Pacific Ocean all play a role in driving GP pluvial events. However, our study extends the validity of these results through analysis of annual reanalysis data spanning over 80 years, a feature lacking

in all other studies. Thus, while we find similar results as the other studies, we advance the understanding of pluvial events by providing a more robust analysis on their occurrences.

Some caveats for this study exist. First, this study relied on composite analyses for distinguishing the associated atmospheric patterns with the pluvial years. Other statistical tools such as empirical orthogonal functions (EOF)/principal component analysis (PCA) could offer other views on the data and the covariability between GP precipitation and geophysical fields. Further investigation using linear and nonlinear methods will be completed as part of our future work in further diagnosing the patterns found in this study. Second, our results are mainly focused on a subset of pluvial years, and as such, the atmospheric patterns identified in our analyses cannot fully explain the occurrence of all pluvial events. The lack of any significant atmospheric signal in pluvial years not included within the Pattern composites highlights the complex nature of the variability of precipitation over the GP. Additionally, the nonpluvial years that were found to meet the criteria for the Pattern composite (EGH anomaly index value over 0.5) need to be further investigated and tested. Determining the reasons why these years matched the pattern found in the Total composite yet did not have excessive precipitation could further enhance the understanding of GP precipitation variability.

Overall, the results of this study bridge the gap between past studies by demonstrating the linkage between the atmospheric patterns contributing to heavy precipitation events and annual GP precipitation variability. Further, pluvial years in the GP are likely more dependent on such atmospheric patterns, rather than the development of anomalous annual precipitation on seasonal or longer time scales. Analysis into the causes of the SGP and NGP patterns is necessary to apply this work to predictability of pluvial years in the GP. This predictability aspect is tied to predicting both the frequency and intensity of storm systems, as both play a role in different regions of the GP. Because of the synoptic nature of these waves, this study also supports the need for more studies in subseasonal-to-seasonal (S2S) forecasting and predictions, an emerging area of importance in the weather and climate communities.

Acknowledgments. The authors thank Dr. Michael Richman at the University of Oklahoma for his contributions to this work. We would also like to thank the anonymous reviewers for their help in refining the work to its current form. This work was supported, in part, by the Agriculture and Food Research Initiative Competitive Grant (2013-69002) from the USDA National Institute of Food and Agriculture and National Science Foundation Grant ICER1663840. ERA-20C data shown in this manuscript are available from http://www.ecmwf.int. NCEP Reanalysis and NOAA CIRES 20th Century Reanalysis data are provided by the NOAA/OAR/ESRL PSD, Boulder, Colorado, from http://www.esrl.noaa.gov/psd/. Japanese 55-year Reanalysis data are available from http://jra.kishou.go.jp/JRA-55/index_en.html.

APPENDIX

List of All Great Plains Pluvial Years

Table A1 contains the list of all pluvial years for the SGP and NGP found in each of the datasets considered.

REFERENCES

Barsugli, J. J., and P. D. Sardeshmukh, 2002: Global atmospheric sensitivity to tropical SST anomalies throughout the Indo-Pacific Basin. *J. Climate*, **15**, 3427–3442, https://doi.org/10.1175/1520-0442(2002)015<3427:GASTTS>2.0.CO;2.

Basara, J. B., J. N. Maybourn, C. M. Peirano, J. E. Tate, P. J. Brown, J. D. Hoey, and B. R. Smith, 2013: Drought and associated impacts in the Great Plains of the United States—A review. *Int. J. Geosci.*, **4**, 72–81, https://doi.org/10.4236/ijg.2013.46A2009.

Branstator, G., and H. Teng, 2017: Tropospheric waveguide teleconnections and their seasonality. *J. Atmos. Sci.*, **74**, 1513–1532, https://doi.org/10.1175/JAS-D-16-0305.1.

Bukovsky, M. S., R. R. McCrary, A. Seth, and L. O. Mearns, 2017: A mechanistically credible, poleward shift in warm season precipitation projected for the U.S. southern Great Plains? *J. Climate*, **30**, 8275–8298, https://doi.org/10.1175/JCLI-D-16-0316.1.

Christian, J., K. Christian, and J. B. Basara, 2015: Drought and pluvial dipole events within the great plains of the United States. *J. Appl. Meteor. Climatol.*, **54**, 1886–1898, https://doi.org/10.1175/JAMC-D-15-0002.1.

Compo, G. P., and Coauthors, 2011: The Twentieth Century Reanalysis Project. *Quart. J. Roy. Meteor. Soc.*, **137**, 1–28, https://doi.org/10.1002/qj.776.

Cook, B. I., R. L. Miller, and R. Seager, 2008: Dust and sea surface temperature forcing of the 1930s ''Dust Bowl'' drought. *Geophys. Res. Lett.*, **35**, L08710, https://doi.org/10.1029/2008GL033486.

——, R. Seager, and R. L. Miller, 2011: On the causes and dynamics of the early twentieth-century North American pluvial. *J. Climate*, **24**, 5043–5060, https://doi.org/10.1175/2011JCLI4201.1.

Daly, C., W. P. Gibson, G. H. Taylor, G. L. Johnson, and P. Pasteris, 2000: High quality spatial climate data sets for the United States and beyond. *Trans. ASAE*, **43**, 1957–1962, https://doi.org/10.13031/2013.3101.

Dore, M. H. I., 2005: Climatic change and changes in global precipitation patterns: What do we know? *Environ. Int.*, **31**, 1167–1181, https://doi.org/10.1016/j.envint.2005.03.004.

Fischer, M. L., D. P. Billesbach, J. A. Berry, W. J. Riley, and M. S. Torn, 2007: Spatiotemporal variations in growing season exchanges of CO_2, H_2O, and sensible heat in agricultural fields of the Southern Great Plains. *Earth Interact.*, **11**, https://doi.org/10.1175/EI231.1.

Flanagan, P. X., J. B. Basara, and X. Xiao, 2017: Long-term analysis of the asynchronicity between temperature and precipitation maxima in the United States Great Plains. *Int. J. Climatol.*, **37**, 3919–3933, https://doi.org/10.1002/joc.4966.

Griffin, K. S., and J. E. Martin, 2017: Synoptic features associated with temporally coherent modes of variability of the North Pacific jet stream. *J. Climate*, **30**, 39–54, https://doi.org/10.1175/JCLI-D-15-0833.1.

Grotjahn, R., and G. Faure, 2008: Composite predictor maps of extraordinary weather events in the Sacramento, California, region. *Wea. Forecasting*, **23**, 313–335, https://doi.org/10.1175/2007WAF2006055.1.

Guo, Y., M. Ting, Z. Wen, D. E. Lee, Y. Guo, M. Ting, Z. Wen, and D. E. Lee, 2017: Distinct patterns of tropical Pacific SST anomaly and their impacts on North American climate. *J. Climate*, **30**, 5221–5241, https://doi.org/10.1175/JCLI-D-16-0488.1.

Hoerling, M., J. Eischeid, A. Kumar, R. Leung, A. Mariotti, K. Mo, S. Schubert, and R. Seager, 2014: Causes and predictability of the 2012 Great Plains drought. *Bull. Amer. Meteor. Soc.*, **95**, 269–282, https://doi.org/10.1175/BAMS-D-13-00055.1.

Hu, Z., and B. Huang, 2009: Interferential impact of ENSO and PDO on dry and wet conditions in the U.S. Great Plains. *J. Climate*, **22**, 6047–6065, https://doi.org/10.1175/2009JCLI2798.1.

llston, B. G., J. B. Basara, and K. C. Crawford, 2004: Seasonal to interannual variations of soil moisture measured in Oklahoma. *Int. J. Climatol.*, **24**, 1883–1896, https://doi.org/10.1002/joc.1077.

Kalnay, E., and Coauthors, 1996: The NCEP/NCAR 40-Year Reanalysis Project. *Bull. Amer. Meteor. Soc.*, **77**, 437–471, https://doi.org/10.1175/1520-0477(1996)077<0437:TNYRP>2.0.CO;2.

Klingaman, N. P., B. Hanson, and D. J. Leathers, 2008: A teleconnection between forced Great Plains snow cover and European winter climate. *J. Climate*, **21**, 2466–2483, https://doi.org/10.1175/2007JCLI1672.1.

Koster, R., M. J. Suarez, and M. Heiser, 2000: Variance and predictability of precipitation at seasonal-to-interannual timescales. *J. Hydrometeor.*, **1**, 26–46, https://doi.org/10.1175/1525-7541(2000)001<0026:VAPOPA>2.0.CO;2.

Livneh, B., and M. P. Hoerling, 2016: The physics of drought in the U.S. central Great Plains. *J. Climate*, **29**, 6783–6804, https://doi.org/10.1175/JCLI-D-15-0697.1.

Mo, K. C., J. Nogues-Paegle, and R. W. Higgins, 1997: Atmospheric processes associated with summer floods and droughts in the central United States. *J. Climate*, **10**, 3028–3046, https://doi.org/10.1175/1520-0442(1997)010<3028:APAWSF>2.0.CO;2.

Moore, R. W., O. Martius, and T. Spengler, 2010: The modulation of the subtropical and extratropical atmosphere in the Pacific basin in response to the Madden–Julian oscillation. *Mon. Wea. Rev.*, **138**, 2761–2778, https://doi.org/10.1175/2010MWR3194.1.

Nieto, R., and Coauthors, 2005: Climatological features of cutoff low systems in the Northern Hemisphere. *J. Climate*, **18**, 3085–3103, https://doi.org/10.1175/JCLI3386.1.

O'Lenic, E. A., D. A. Unger, M. S. Halpert, and K. S. Pelman, 2008: Developments in operational long-range climate prediction at CPC. *Wea. Forecasting*, **23**, 496–515, https://doi.org/10.1175/2007WAF2007042.1.

Onogi, K., and Coauthors, 2007: The JRA-25 Reanalysis. *J. Meteor. Soc. Japan*, **85**, 369–432, https://doi.org/10.2151/jmsj.85.369.

Pal, J. S., and E. A. B. Eltahir, 2002: Teleconnections of soil moisture and rainfall during the 1993 Midwest summer flood. *Geophys. Res. Lett.*, **29**, 1865, https://doi.org/10.1029/2002GL014815.

Pederson, N., A. R. Bell, E. R. Cook, U. Lall, N. Devineni, R. Seager, K. Eggleston, and K. P. Vranes, 2013: Is an epic pluvial masking the water insecurity of the greater New York City region? *J. Climate*, **26**, 1339–1354, https://doi.org/10.1175/JCLI-D-11-00723.1.

Poli, P., and Coauthors, 2016: ERA-20C: An atmospheric reanalysis of the twentieth century. *J. Climate*, **29**, 4083–4097, https://doi.org/10.1175/JCLI-D-15-0556.1.

Randall, D., 2015: *An Introduction to the Global Circulation of the Atmosphere.* Princeton University Press, 456 pp.

Rosenzweig, C., A. Iglesias, and X. Yang, 2001: Climate change and extreme weather events: Implications for food production, plant diseases and pests. *Global Change Hum. Health*, **2**, 90–104, https://doi.org/10.1023/A:1015086831467.

Ruiz-Barradas, A., and S. Nigam, 2005: Warm season rainfall variability over the U.S. Great Plains in observations, NCEP and ERA-40 reanalyses, and NCAR and NASA atmospheric model simulations. *J. Climate*, **18**, 1808–1830, https://doi.org/10.1175/JCLI3343.1.

Schubert, S. D., M. J. Suarez, P. J. Pegion, R. D. Koster, and J. T. Bacmeister, 2004: Causes of long term drought in the U.S. Great Plains. *J. Climate*, **17**, 485–503, https://doi.org/10.1175/1520-0442(2004)017<0485:COLDIT>2.0.CO;2.

——, ——, ——, ——, and ——, 2008: Potential predictability of long-term drought and pluvial conditions in the U.S. Great Plains. *J. Climate*, **21**, 802–816, https://doi.org/10.1175/2007JCLI1741.1.

Seager, R., and M. P. Hoerling, 2014: Atmosphere and ocean origins of North American droughts. *J. Climate*, **27**, 4581–4606, https://doi.org/10.1175/JCLI-D-13-00329.1.

——, N. Harnik, W. A. Robinson, Y. Kushnir, M. Ting, H. P. Huang, and J. Velez, 2005: Mechanisms of ENSO-forcing of hemispherically symmetric precipitation variability. *Quart. J. Roy. Meteor. Soc.*, **131**, 1501–1527, https://doi.org/10.1256/qj.04.96.

——, L. Goddard, J. Nakamura, N. Henderson, and D. E. Lee, 2014: Dynamical causes of the 2010/11 Texas–northern Mexico drought. *J. Hydrometeor.*, **15**, 39–68, https://doi.org/10.1175/JHM-D-13-024.1.

Seo, H., Y. Kwon, T. M. Joyce, and C. C. Ummenhofer, 2017: On the predominant nonlinear response of the extratropical atmosphere to meridional shifts of the Gulf Stream. *J. Climate*, **30**, 9679–9702, https://doi.org/10.1175/JCLI-D-16-0707.1.

Ting, M., and H. Wang, 1997: Summertime U.S. precipitation variability and its relation to Pacific sea surface temperature. *J. Climate*, **10**, 1853–1873, https://doi.org/10.1175/1520-0442(1997)010<1853:SUSPVA>2.0.CO;2.

Trenberth, K. E., and G. W. Branstator, 1992: Issues in establishing causes of the 1988 drought over North America. *J. Climate*, **5**, 159–172, https://doi.org/10.1175/1520-0442(1992)005<0159:IIECOT>2.0.CO;2.

——, and C. J. Guillemot, 1996: Physical processes involved in the 1988 drought and 1993 floods in North America. *J. Climate*, **9**, 1288–1298, https://doi.org/10.1175/1520-0442(1996)009<1288:PPIITD>2.0.CO;2.

Weaver, S., S. Baxter, and K. Harnos, 2016: Regional changes in the interannual variability of warm season precipitation. *J. Climate*, **29**, 5157–5173, https://doi.org/10.1175/JCLI-D-14-00803.1.

Westerling, A. L., A. Gershunov, T. J. Brown, D. R. Cayan, and M. D. Dettinger, 2003: Climate and wildfire in the western United States. *Bull. Amer. Meteor. Soc.*, **84**, 595–604, https://doi.org/10.1175/BAMS-84-5-595.

——, H. G. Hidalgo, D. R. Cayan, and T. W. Swetnam, 2006: Warming and earlier spring increase western US forest wildfire activity. *Science*, **313**, 940–943, https://doi.org/10.1126/science.1128834.

Wilhelmi, O. V., and D. A. Wilhite, 2002: Assessing vulnerability to agricultural drought: A Nebraska case study. *Nat. Hazards*, **25**, 37–58, https://doi.org/10.1023/A:1013388814894.

Wilhite, D. A., 2000: Drought as a natural hazard: Concepts and definitions. *Droughts: A Global Assessment*, D. A. Wilhite, Ed., Routledge, 3–18.

Wuebbles, D., and Coauthors, 2014: CMIP5 climate model analyses: Climate extremes in the United States. *Bull. Amer. Meteor. Soc.*, **95**, 571–583, https://doi.org/10.1175/BAMS-D-12-00172.1.

Yang, S., X. Ding, D. Zheng, and Q. Li, 2007: Depiction of the variations of Great Plains precipitation and its relationship with tropical central-eastern Pacific SST. *J. Appl. Meteor. Climatol*, **46**, 136–153, https://doi.org/10.1175/JAM2455.1.

Yin, D., M. L. Roderick, G. Leech, F. Sun, and Y. Huang, 2014: The contribution of reduction in evaporative cooling to higher surface air temperatures during drought. *Geophys. Res. Lett.*, **41**, 7891–7897, https://doi.org/10.1002/2014GL062039.

Zhao, S., Y. Deng, and R. Black, 2017: A dynamical and statistical characterization of U.S. extreme precipitation events and their associated large-scale meteorological patterns. *J. Climate*, **30**, 1307–1326, https://doi.org/10.1175/JCLI-D-15-0910.1.